HHS Public Access

Author manuscript

Nat Med. Author manuscript; available in PMC 2014 June 01.

Published in final edited form as:

Nat Med. 2013 December ; 19(12): 1632–1637. doi:10.1038/nm.3393.

CD28 and ITK signals regulate autoreactive T cell trafficking

Nitya Jain[1], **Bing Miu**[1], **Jian-kang Jiang**[2], **Kai K. McKinstry**[1], **Amanda Prince**[1], **Susan L Swain**[1], **Dale L. Greiner**[3], **Craig J. Thomas**[2], **Michael J. Sanderson**[4], **Leslie J Berg**[1], and **Joonsoo Kang**[1]

[1]Department of Pathology, University of Massachusetts Medical School, 55 Lake Avenue North, Worcester, MA 01655, USA.

[2]National Institutes of Health, NIH Chemical Genomics Center, 9800 Medical Center Drive, Rockville, MD 20850, USA

[3]Program in Molecular Medicine, University of Massachusetts Medical School, Worcester, MA 01655 USA.

[4]Microbiology and Physiological Systems, University of Massachusetts Medical School, Worcester, MA 01655 USA.

Abstract

Activation of self-reactive T cells and their trafficking to target tissues leads to autoimmune organ destruction. Mice lacking the coinhibitory receptor CTLA-4 develop fatal autoimmunity characterized by massive lymphocytic invasion into non-lymphoid tissues. Here we demonstrate that the CD28 costimulatory pathway regulates the trafficking of self-reactive *Ctla4*$^{-/-}$ T cells to tissues. Co-ablation of the CD28-activated Tec family kinase ITK does not block spontaneous T cell activation, but instead causes self-reactive *Ctla4*$^{-/-}$ T cells to accumulate in secondary lymphoid organs. Despite a fulminant autoimmune process in the lymphoid compartment, *Itk*$^{-/-}$*Ctla4*$^{-/-}$ mice are otherwise healthy and exhibit a long lifespan. We propose that ITK licenses autoreactive T cells to enter tissues to mount destructive immune responses. Importantly, ITK inhibitors mimic the null mutant phenotype and also prevent pancreatic islet infiltration by diabetogenic T cells in mouse models of Type I diabetes, highlighting their potential utility for the treatment of human autoimmune disorders.

CD28 is the primary costimulatory molecule for naive CD4^{+} conventional T (Tconv) cell activation[1]. CD28 binding to B7 ligands leads to increased duration and magnitude of T cell responses[2], enhanced survival and glucose metabolism[3], [4] and acquisition of migratory properties[5]. CD28 activates integrin-mediated adhesion of T cells[6] and promotes actin polymerization[7,8]. *Cd28*$^{-/-}$ mice have impaired delayed-type hypersensitivity responses[9] and fail to develop Experimental Autoimmune Encephalitis (EAE)[10],[11]. In non-obese

Author Contributions

NJ, LB and JK designed experiments, NJ and BM performed experiments and analyzed data, KM and SS conducted Flu infection studies, AP performed LCMV infections, JJ and CT prepared ITK inhibitors, DG provided reagents for T1D experiments, MS collaborated on fluorescence microscopy, NJ and JK wrote the manuscript, JK and LB supervised the project.

diabetic (NOD) mice, loss of CD28 exacerbates Type 1 diabetes (T1D)[12], likely due to decreased frequency of FOXP3$^+$ Treg cells[13]. However, NOD mice treated with CTLA4Ig (Abatacept), a protein that binds to and sequesters B7, are protected from diabetes[14]. Interpretations of these studies are complicated by the function of the CD28 antagonist, CTLA-4, that binds B7 with a much higher affinity than CD28[15,16].

CTLA-4 maintains T cell tolerance to self[15], and polymorphisms in *Ctla4* have been linked to human autoimmune diseases[17]. *Ctla4*$^{-/-}$ mice die of a lymphoproliferative disorder driven by rampant CD28-dependent self-reactive CD4$^+$ T cell activation and infiltration into tissues[18,19]. This loss in tolerance is initiated by the inability of CTLA-4-deficient Treg cells to function[19-22], resulting in hyper-stimulatory antigen presenting cells[20,21]. CTLA-4 also has Tconv cell-intrinsic functions and regulates trafficking of self-reactive T cells[19,22]. Expression of a truncated CTLA-4 containing only the B7-binding domain protects *Ctla4*$^{-/-}$ mice from organ infiltration by T cells[23]. These results suggest that modulation of CD28 signals by competitive sequestration of B7 ligands can regulate tissue infiltration by autoreactive T cells.

Studies have suggested the involvement of CD28-activated PI3Kinase (PI3K) in the trafficking of effector T cells to tissues[24,25]. The IL-2 inducible Tec kinase ITK is recruited to both the TCR and CD28 upon stimulation in a PI3K-dependent manner[26]. Phosphorylated ITK activates PLC-ρ1, leading to calcium (Ca^{2+}) mobilization and actin polarization to the site of TCR stimulation[27]. ITK is also activated by β1-integrins and is involved in Cdc42 and Rac mediated chemokine-induced migration[28,29]. However, CD28 and ITK appear dispensable for T cell localization to target tissues in inflammatory settings[16, 30]. Here, we show that CD28-ITK signals specifically regulate self-reactive T cell migration in tissues. Importantly, small molecule inhibitors of ITK significantly diminished T cell infiltration and destruction of islet cells in T1D models, providing proof of principle that targeting ITK may be beneficial for treating T cell-mediated human organ-specific autoimmune diseases.

Results

Ctla4$^{-/-}$ T cell migration to tissues requires CD28-B7 signals

Ctla4$^{-/-}$ CD4$^+$ T cells recognize tissue self-antigens and represent a model of multi-organ autoimmunity. Mice deficient in both *Cd28* and *Ctla4* are protected from lethal autoimmunity since T cells cannot be activated[31]. Further, CD28 signals were necessary for tissue infiltration by self-reactive T cells as transfer of *Ctla4*$^{-/-}$ lymph node (LN) T cells into B7-sufficient *Rag1*$^{-/-}$ mice instigated an aggressive autoimmune disease similar to intact *Ctla4*$^{-/-}$ mice, but transfer into B7$^{-/-}$*Rag1*$^{-/-}$ mice did not (**Fig. 1a**). Transfer of *Ctla4*$^{-/-}$ T cells into MHC Class II-deficient *Rag1*$^{-/-}$ mice resulted in an intermediate disease course with 75% of mice displaying tissue infiltrates (**Supplementary Fig. 1a**). These results suggested a more stringent requirement for CD28 than TCR-MHC class II signals for activated *Ctla4*$^{-/-}$ T cell accumulation in tissues.

Endothelial cells (ECs) in LNs express some B7 and MHC class II molecules, [32-35]. We determined the expression of B7 on stromal subsets in the lungs (**Supplementary Fig. 1b**). CD86 was expressed on CD45$^+$ hematopoietic cells, and at low but significant amounts on

CD45^{neg} stromal cells (**Supplementary Fig. 1c**). Imaging studies also identified a CX3CR1^{+} DC population on vessel walls of lungs that projected dendrites into the lumen ([36] and **data not shown**). These results suggested that B7 molecules in tissues are accessible to blood-borne T cells. *In vitro*, B7-CD28 signals were required for the migration of activated *Ctla4*$^{-/-}$ T cells across B7^{+} SVEC4-10 ECs[34,37], as neutralizing B7 antibodies curtailed their migration (**Supplementary Fig. 1d**).

We next performed 2-photon imaging of fluorescently labeled *Ctla4*$^{-/-}$ T cells in lung vasculature[38,39] of WT and B7-deficient mice to characterize their motility. *Ctla4*$^{-/-}$ T cells in WT mice were highly motile within blood vessels in lung slices, made frequent stable contacts with, and often migrated across, vessel walls (**Supplementary Movie 1, Fig. 1b**). They showed significant mean displacement within the time frame of recording (**Fig. 1c, d**) and had the characteristic elongated morphology of migrating cells (**Fig. 1b, e**). In contrast, *Ctla4*$^{-/-}$ T cells in *ex vivo* B7$^{-/-}$ lung tissues did not make stable contact with ECs, lost directionality and assumed a circular morphology (**Fig. 1b-e; Supplementary Movie 2**). These results indicated that CD28-B7 interactions modulate *Ctla4*$^{-/-}$ T cell trafficking in tissues.

ITK deficiency prevents lethality of *Ctla4*$^{-/-}$ mice

To identify a CD28 signaling molecule required for T cell trafficking, we focused on ITK. To confirm that ITK functions downstream of CD28, we stimulated naïve WT and *Itk*$^{-/-}$ CD4^{+} T cells with a CD28 super-agonist (SACD28) antibody[40] that can trigger T cell activation without overt TCR signaling. WT naïve T cells responded to SACD28 crosslinking by up-regulating activation markers CD25 and CD69, but *Itk*$^{-/-}$ CD4^{+}T cells failed to do so (**Supplementary Fig. 1e**).

We then generated *Itk*$^{-/-}$*Ctla4*$^{-/-}$ double knockout (DKO) mice to test if ITK functions in self-reactive T cell trafficking. Unlike *Ctla4*$^{-/-}$ mice that die by 3-4 weeks of age of multi-organ autoimmunity, DKO mice were healthy and had a significantly extended life span (**Fig. 2a**). Yet, DKO mice had engorged LNs **(Fig. 2b),** 20 times larger than those of normal mice, packed with proliferating (Ki67^{+}), activated (CD44^{hi}CD62L^{lo}) T cells (**Fig. 2b, c)** that were fully capable of effector cytokine production (**Supplementary Fig. 2a**), and comparable to *Ctla4*$^{-/-}$ T cells in apoptosis (**Supplementary Fig. 2b**). These results indicated that ITK signaling was not required for the activation of *Ctla4*$^{-/-}$ T cells. Consistent with this, naive CD4^{+} T cells from *5C.C7*Tg*Itk*$^{-/-}$*Ctla4*$^{-/-}$*Rag1*$^{-/-}$ mice responded normally to the cognate antigen (**Supplementary Fig. 2c**). Lastly, global gene expression profiling of CD4^{+} T cells from *Ctla4*$^{-/-}$ and DKO mice showed that these two populations were molecularly convergent, with less than 0.5% of genes differentially expressed (**Supplementary Fig 2d**), supporting the conclusion that the activation and functional states of *Ctla4*$^{-/-}$ T cells were not impaired by the loss of ITK.

Lack of autoimmune tissue pathology in *Itk*$^{-/-}$*Ctla4*$^{-/-}$ mice

While DKO mice exhibited an increased frequency of Treg cells in SLOs (**Fig. 2c**), the lack of CTLA-4 rendered these Treg cells functionally impaired, as they were unable to regulate colitogenic naïve WT T cells *in vivo* (**Supplementary Fig 2e**). Further, in the presence of

WT Treg cells in mixed bone marrow chimeras, DKO T cells were prevented from activation (**Supplementary Fig. 2f**), showing that the rampant T cell expansion in DKO mice was caused by the lack of CTLA-4 on Treg cells [21].

Despite defective Treg cells and lymphoproliferation, DKO mice did not exhibit autoimmune tissue infiltration histologically (**Fig. 3a**). The few T cells present in tissues of older DKO mice did not exhibit differences in cell survival (**Supplementary Fig. 2b**). The compromised tissue infiltration by DKO T cells was a cell-intrinsic defect, as reconstitution of *Tcrb*$^{-/-}$ mice with DKO T cells did not cause diesease, whereas transferred *Ctla4*$^{-/-}$ T cells caused lethal autoimmunity (**Fig. 3b**). Pertussis toxin (PTx) facilitates the movement of autoreactive T cells to brain tissues to induce EAE in mice[41]. Treatment of DKO mice with PTx led to a rapid wasting disease with death starting in one month (**data not shown**). Consistently, there were increased lymphocytic infiltrates into organs accompanied by robust effector cytokine production by CD4^{+} T cells (**Fig. 3c**). Importantly, DKO mice could mount effective anti-viral T cell responses in tissues and clear infections with the A/PR8 strain of Influenza A and LCMV Armstrong viruses similar to controls (**Supplementary Fig. 2g, h**). These results indicated that DKO T cells are not irreversibly excluded from tissues, and that ITK appears to only license aberrantly activated, self-reactive T cells to accumulate in tissues.

Chemokine responses and tissue homing of *Itk*$^{-/-}$*Ctla4*$^{-/-}$ T cells

Gene expression and flow cytometry assays revealed no significant differences in the expression of adhesion molecules and most chemokine receptors between *Ctla4*$^{-/-}$ and DKO T cells (**Supplementary Fig. 3a, b**). RNA analysis showed similar expression of the S1P receptor, important for LN egress, and comparable migration to S1P ligand by *Ctla4*$^{-/-}$ and DKO T cells (**Supplementary Fig. 3c**). Increased numbers of CD4^{+} T cells in blood of DKO mice further indicated that DKO T cells can exit the LNs (**Supplementary Fig. 3d**). Of note, however, were the decreased expression of CXCR3[42] on activated DKO CD4^{+} T cells and their failure to migrate to CXCL-11 *in vitro* (**Supplementary Fig. 4a, b**). However, while *Cxcr3*$^{-/-}$*Ctla4*$^{-/-}$ mice displayed a small but significant extension in lifespan relative to *Ctla4*$^{-/-}$ mice, massive lymphocytic infiltrates were still evident in most organs (**Supplementary Fig. 4c, d**). Thus, reduced expression of CXCR3 on DKO CD4^{+} T cells likely contributes to, but cannot fully account for the paucity of DKO T cells in tissues.

To determine whether DKO T cells are selectively impaired in migration to tissues, we performed a competitive short-term homing assay of DKO and *Ctla4*$^{-/-}$ T cells in *Rag1*$^{-/-}$ mice. At 6-8 hours post-transfer, the cells remained undivided and there was no difference in the expression of apoptosis marker AnnexinV in tissues (**Supplementary Fig. 4e**). In the lungs and liver, the normalized ratios of DKO/*Ctla4*$^{-/-}$ CD4^{+} and CD8^{+} T cells (homing index; HI), was <1.0 (**Fig. 4a; Supplementary Fig. 4e**), indicating a significant advantage of *Ctla4*$^{-/-}$ T cells in repopulating these tissues. Reciprocally, a HI of >1.5 in the LNs indicated an enhanced accumulation of DKO T cells in lymphoid tissues. The difference was observed regardless of initial input ratios ranging from 2:1 to 1:4 of *Ctla4*$^{-/-}$:DKO cells (**data not shown**). These results indicate that in this short time frame, DKO T cells do not migrate to non-lymphoid tissues as efficiently as *Ctla4*$^{-/-}$ T cells.

Itk$^{-/-}$*Ctla4*$^{-/-}$ T cells are defective in trans-endothelial migration

Morphological changes enable T cells to traffic across ECs from the blood to tissues[43]. Activated DKO CD4$^+$ T cells had impaired F-actin polarization relative to *Ctla4*$^{-/-}$ T cells *ex vivo* (**Fig. 4b, Supplementary Fig. 3e**). Further, unlike *Ctla4*$^{-/-}$ T cells, a significantly lower frequency of DKO CD4$^+$ T cells was able to migrate across an EC layer *in vitro* (**Fig. 4c**). Pre-treatment of DKO T cells with a Ca^{2+} ionophore that can partly substitute for CD28 signaling increased the frequency of DKO T cells that were able to migrate across the endothelium (**Supplementary Fig. 3f**). Similarly, migration of *Ctla4*$^{-/-}$ T cells across ECs *in vitro* was blocked by an ITK inhibitor[44] (**Supplementary Fig. 3g**).

Two-photon imaging of DKO lymphocytes in lung slices showed that, in contrast to *Ctla4*$^{-/-}$ T cells, DKO T cells exhibited a random movement within blood vessels in lung tissue and were morphologically distinct (**Fig. 4d-g**; **Supplementary Movie 3, 4**). The migratory properties of DKO cells were strikingly similar to that of *Ctla4*$^{-/-}$ T cells in B7$^{-/-}$ lung slices (**Fig. 1**), suggesting that impaired CD28 signaling in DKO T cells was responsible for the observed defects.

ITK inhibitors moderate autoimmunity

Data in aggregate suggested that pharmacological inhibition of ITK might moderate autoimmune disease pathogenesis. Treatment of *Ctla4*$^{-/-}$ mice with two ITK inhibitors, BMS509744[45] and 10n[46], significantly increased their lifespan (**Fig. 5a**). The inhibition of ITK did not alter the activation state or proliferative capacity of *Ctla4*$^{-/-}$ T cells (**Supplementary Fig. 5a**), but led to a significant increase in the size of LNs **(Supplementary Fig. 5b**), consistent with earlier genetic studies (**Fig. 2b, c**). However, despite the increased longevity, lymphocytic infiltration was observed in most tissues (**data not shown**). This result was not unexpected given the relatively poor pharmacokinetics of the ITK inhibitors, combined with the rapid-onset, destructive disease in *Ctla4*$^{-/-}$ mice.

We next tested the ability of ITK inhibitors to prevent β-islet infiltration in NOD mice. Administration of 10n to female NOD mice caused an increase in the cellularity of the LNs (**Supplementary Fig. 5c**). Notably, 10n treatment reduced the migration of self-reactive T cells into β-islets of NOD mice by 50% (**Fig. 5b, c**). Given the prohibitive amount of 10n required for long-term studies in NOD mice, we instead chose to examine whether 10n could block diabetogenic BDC2.5/NOD CD4$^+$ T cells from causing islet cell destruction. Transfer of BDC2.5/NOD CD4$^+$CD25^{neg} T cells into young NOD/*Scid* mice[47], with parallel 10n treatment moderated insulitis (**Fig. 5d**) and diminished the onset of diabetes (**Fig. 5e**).

Discussion

CTLA-4 and CD28 are critical for regulating autoimmunity such as T1D, but are often dispensable for responses against foreign pathogens[12,21,48,49]. Most *in vivo* studies support the role of ligand competition as the primary mode of CTLA-4 inhibition of CD28 signals[23,50-53]. We show here that CD28-B7 interactions and ITK regulate the trafficking of self-reactive T cells to tissues, but are not essential for pathogen clearance[54]. Given the established biochemical connection between CD28 and ITK, these data support the model

that one Tconv cell-intrinsic function of CTLA-4 is to modulate the CD28-ITK pathway controlling self-reactive T cell motility in tissues.

We showed that ITK inhibitors are effective in treating T1D in mice. Costimulatory blockade is a major therapeutic strategy for autoimmune diseases such as rheumatoid arthritis and T1D. Abatacept, a CD28 antagonist, has achieved moderate success in T1D patients, leading to the preservation of beta-cell mass for over two years[55]. However, this approach ultimately fails due to the increased antigen sensitivity of autoreactive T cells, and their relative independence from costimulation for their activation. Another major drawback is the failure to specifically target auto-reactive T cells as the B7 blockade can interfere with Treg cell function[13]. In contrast, focused approaches aimed at regulating self-reactive T cell migration to organs to limit immune pathology are beneficial in treating severe autoimmunity[56]. ITK has been shown to have a similar functional repertoire in human T cells as in mice[44,57,58]. Our data indicate that ITK inhibitors can become an alternate strategy to treat diverse human T cell mediated organ-specific autoimmune diseases, while allowing pathogen-elicited immune responses to occur.

Online Methods

Mice

Itk$^{-/-}$ mice were crossed with *Ctla4*$^{-/-}$ mice to generate *Itk*$^{-/-}$*Ctla4*$^{-/-}$ (DKO) mice on the C57/BL6 background. Female NOD, NOD/Scid mice, *Cxcr3*$^{-/-}$ and *Cd80*$^{-/-}$*Cd86*$^{-/-}$ (B7$^{-/-}$) mice were purchased from Jackson Laboratories (Bar Harbor, ME). BDC2.5/NOD mice were bred in our animal facility. *Cd80*$^{-/-}$*Cd86*$^{-/-}$*Rag1*$^{-/-}$ and 5C.C7*Itk*$^{-/-}$*Ctla4*$^{-/-}$*Rag1*$^{-/-}$ mice were generated in our colony. *Rag1*$^{-/-}$*H-2Aa*$^{-/-}$*Cd74*$^{-/-}$ (no I-A, E; MHC Class II$^{-/-}$) mice were provided by Dr. Huseby. All experiments were approved by the University of Massachusetts Medical School Institutional Animal Care and Use Committee.

Reagents, antibodies, flow cytometry and histology

Pertussis toxin was from List Biological Laboratories, Campbell CA; ITK inhibitors, BMS507944 and 10n, were synthesized at the NIH's Chemical Genomics Centre and dissolved in 70% (20%w/v) 2-hydroxypropyl-B-cyclodextrin in water and 30% PEG300 (EMD), CD28 superagonist antibody (SACD28, clone D665) was a gift from Dr. T Hunig and S1P was from R&D Systems. Most antibodies used in these experiments were purchased from BD Bioscience (San Jose, California) and eBioscience (San Diego, CA) (**Supplementary Table 1**). All data were acquired on the LSRII flow cytometer (BD), and analyzed using FlowJo software (Treestar, CA). Peripheral T cell subsets were sorted to greater than 95% purity using a MoFlo (Cytomation) cell sorter. CD4^{+}T cells were enriched from SLOs by depleting CD8^{+} T cells and B220^{+} T cells using MACS (Miltenyi Biotec) beads according to the manufacturer's protocol. For histology, organs were fixed in 10% formalin. Four microns paraffin embedded sections were cut and stained with hematoxylin and eosin (H&E). Minimally, 4 sections at multiple depths were analyzed.

In vitro T cell activation and migration assays

5×10^5 naïve $CD4^+$ T cells from 5C.C7*Rag1*$^{-/-}$ mice were stimulated with indicated concentrations of $MCC_{88\text{-}103}$ (moth cytochrome c) pulsed CHO cells expressing MHC class II, I-E^k, with or without scFvCD28 (variable fragment of CD28 antibody expressed as a trans-membrane protein on CHO cell surface). FACS sorted naive ($CD4^+CD8^-CD19^-CD11c^-CD25^-CD62L^+CD44^{lo}$) $CD4^+$T cells from WT and *Itk*$^{-/-}$ mice were stimulated with 10μg ml^{-1} SACD28 antibody at 37ºC for 24 hours, with recombinant IL-4 (2ng ml^{-1}, R&D Systems) in some cultures. DKO LN cells were stimulated with 2μg ml^{-1} Ionomycin for 2 hours prior to trans-endothelial migration assay. *Ctla4*$^{-/-}$ LN cells were pre-incubated with ITK inhibitor, 10n (10μg ml^{-1}), for 2 hours prior to trans-endothelial migration assay. Intra-cellular cytokine staining was performed after stimulating cells with PMA (50ng ml^{-1}) and Ionomycin (750ng ml^{-1}) for 4 hours in the presence of Golgi Stop and Plug (BD Bioscience). For trans-endothelial migration assays, a monolayer of SVEC4-10 (ATCC-CRL-2181; characterized as lymphatic, HEV, or blood microvascular endothelium) ECs was established on the underside of a trans-well insert such that the migrating lymphocytes would first contact the basal surface of the endothelium, recapitulating migration *in vivo*, as previously described[37]. Briefly, 100μl of 0.1% Gelatin was added to the underside of trans-well insert and incubated for 2 hours at 37ºC. The gelatin was then discarded and 5×10^4 SVEC4-10 cells in 50μl complete media were added to the inverted insert. The set-up was incubated for 72 hours at 37ºC. Confluency of cells was determined by staining insert with the cytosolic dye, CFSE, and visualizing under a fluorescence microscope. Where indicated, monolayers were stimulated with 25ng ml^{-1} of TNFα for 24 hours, after which MACS purified $CD4^+$ T cells were added to the upper chamber. The frequency of migrated cells was determined after 4 hours of incubation at 37ºC.

Short-term migration assays

Cells from LNs and spleen of 3-4 weeks old DKO and *Ctla4*$^{-/-}$ mice (both sexes) were labeled with CFSE and eFluor670, respectively, mixed at different ratios and 30×10^6 cells were intravenously injected into age-matched, non-irradiated *Rag1*$^{-/-}$ mice. 6-8 hours after transfer, peripheral blood lymphocytes were collected via tail bleed. Mice were then euthanized and lymphocytes isolated from perfused lungs and liver by collagenase digestion, as well as from SLOs. Frequencies of $CD4^+$ and $CD8^+$ T cells ($TCR\beta^+$ or $Thy1^+$) were determined by flow cytometry in each tissue.

Treg cell assays

To generate mixed bone marrow chimeras (BMC), BM cells were flushed from the femurs and tibias of donor mice and depleted of $CD4^+$ and $CD8^+$ T cells using magnetic Dynal beads (Invitrogen). 5×10^6 BM cells were injected into lightly irradiated (300 rads) *Rag1*$^{-/-}$ ($Ly5.2^+$) mice via the tail vein. $Ly5.1^+$ *wt* BM was used for control experiments to verify normal reconstitutions. Mice were bled periodically to determine reconstitution of the peripheral T cell pool. Mice were sacrificed and analyzed at >8 wks post transfer. For colitis assays, 2×10^5 sorted $CD4^+CD25^+$ Treg cells were co-transferred with 5×10^5 WT $CD4^+$ Tconv cells into *Rag1*$^{-/-}$ mice. Mice were weighed weekly and examined for signs of colitis

and wasting. Histological examination of colons was performed 6 weeks after adoptive transfer for transmural inflammation and leukocyte infiltration.

Viral infections

Age and sex-matched mice were infected with 5×10^4 PFU of LCMV Armstrong intraperitoneally. To measure relative viral load, mice were euthanized at d11 post-infection, spleens removed and halved prior to homogenizing in 1 mL of RPMI complete media. RNA was isolated using TRIzol reagent and reverse-transcribed according to manufacturer's protocol. Real-time quantitative PCR was performed on the glycoprotein (GP) of LCMV and 18sRNA as previously described[59]. To track T cell responses infected mice were analyzed at various times by flow cytometry using viral epitope-specific MHC Class I tetramers and intracellular cytokine production. For Influenza A virus, age and sex-matched mice were infected intra-nasally under light isoflurane anesthesia with 2,500 Egg Infectious Doses 50 (EID_{50}) of A/PR8 strain of influenza A virus in 50μl of PBS. Mice were weighed every day and euthanized at d18 post-infection. Viral titres were determined at d7 and 14 post-infection by quantifying viral RNA as previously described[60].

Gene expression profiling

$CD4^+CD25^{neg}$ T cells from 3 weeks old male *Ctla4*$^{-/-}$ or DKO mice were sorted in duplicates, RNA was extracted using TRIzol reagent and microarray analysis performed with the Affymetrix MoGene 1.0 ST array based on the ImmGen protocol (http://www.immgen.org/Protocols/Total RNA Extraction with Trizol.pdf). Data were analyzed with modules of the GenePattern genomic analysis platform of the Broad Institute (http://www.broadinstitute.org/ cancer/software/genepattern). Differences in gene expression were identified by the Multiplot module (coefficient of variation <0.5; P value ≤0.05, Student's t-test; expressed genes defined as those with mean expression value > 120 in at least one sample, 95% confidence interval, based on Immgen.org data processing of the MoGene 1.0 ST arrays) and functional categorization was performed using the Functional Annotation Tool DAVID for GO annotations. Heat maps were generated by row (gene) based hierarchical clustering (pairwise complete linkage) of data using the HierarchicalClustering module. Data were log transformed and row centered (subtraction from the mean) and a relative color scale based map generated using the HierarchicalClusteringViewer module. Microarray data deposition to GEO is in progress.

Confocal Microscopy and Immunofluorescence

2×10^6 MACS enriched $CD4^+$ T cells were fixed in 4% para-formaldehyde and permeabilized in 0.15% saponin and stained for actin with phalloidin-488 (5 Units, Invitrogen). Images were captured using a Nikon Eclipse E 600 microscope and IPlab Spectrum software (Scanalytics, VA). At least 15 fields were photographed and no less than 100 cells per sample were analyzed for each experiment. For confocal microscopy, $CD4^+$ T cells were photographed using a Leica confocal microscope.

Preparation of lung slices for microscopy

The procedure was performed as described[39] with some modifications. Briefly, mice were intravenously injected with 50μM of CMTMR Orange dye (Invitrogen). After 30 minutes, 20-50 × 10^6 CFSE (Invitrogen) labeled LN cells were intravenously injected and mice euthanized 5 minutes later. The trachea was cannulated, and lungs inflated with 0.9-1.3ml of 1.8% LMP agarose in sHBSS (HBSS+20mM HEPES, pH 7.4). The agarose was gelled and a lung lobe was cut into 200μm thick serial sections. Lung slices were adhered to a glass bottom dish (In vitro Scientific) by serial additions of a thin film of 2% agarose and bathed in 2 ml of phenol-red free DMEM containing HEPES and 10% FBS. Microscopy was performed at 35°C.

Fluorescence microscopy

Fluorescence imaging was performed using a custom-built 2-photon or confocal microscope using a 40X or 60X objective with numerical apertures of 1.35 or 1.42, respectively. Cells were excited at 820 nm for 2-photon microscopy, and at 488 nm and 543 nm for confocal microscopy. Simultaneous fluorescence images were collected by separating the emitted fluorescence light with a 540 nm dichroic mirror in conjunction with a red (590 nm) and green (510 nm) barrier filter (Semrock). No substantial differences in the data were observed between the 2 microscopes. To follow lymphocyte motility, a time-lapse 2D image sequence was acquired by averaging 16 images (480 × 800 pixels at 15 images/second) every 5 seconds using Video Savant software (IO Industries). Each average image had dimensions of 240 μm × 288 μm with a pixel resolution of 0.5 × 0.36 μm using a 40x objective. Data was analyzed using both Video Savant and Image J (NIH) software. Various descriptors of lymphocyte motility (displacement, roundness) were calculated using ImageJ software.

Diabetes induction and calculation of insulitis index

5 weeks old female NOD mice were treated with ITK inhibitor as indicated and extent of insulitis was determined by histopathological analysis of pancreatic sections. For T cell transfer experiments, 1 × 10^6 sorted $CD4^+CD25^{neg}$ conventional T cells from 4 weeks old female BDC2.5/NOD TCR Tg mice were i.v. injected into 4wks old female NOD/scid mice. Mice were considered diabetic if they had 3 consecutive blood glucose readings of >250mg dL^{-1}. Insulitis index was calculated by scoring the islets as Grade 0: No infiltration; Grade 1: Peri-insulitis only; Grade 2: <20% of islet mass infiltrated; Grade 3: 75% of islet mass infiltrated; Grade 4: <20% of islet mass remaining as determined by insulin immuno-histochemistry. Insulitis index was calculated using the formula: I=(0×N0)+(1×N1)+(2×N2)+(3×N3)+(4×N4)/ (N0+N1+N2+N3+N4); where N0, N1, N2, N3 and N4 are the number of islets showing Grade 0, 1, 2, 3 and 4 pathology respectively.

ITK inhibitor characterization and purification

10n: ^{1}H NMR (400 MHz, DMSO-d_6) δ 13.14-13.00 (br.s., 1H), 8.24-8.11 (br.s., 1H), 7.92-7.79 (br.s., 1H), 7.63 (d, J= 3.8 Hz, 1H), 7.52 (s, 1H), 7.49 (d, J= 8.4 Hz, 1H), 7.22 (d, J= 3.8 Hz, 1H), 7.20 (dd, J= 8.4, 1.0 Hz, 1H), 5.03 (s, 1H), 4.14 (s, 2H), 3.91 (d, J= 12.7 Hz, 1H); 3.66 (d, J= 12.7 Hz, 1H), 2.20 (q, J= 6.4 Hz, 1H), 1.23 (s, 6H), 0.95 (d, J= 6.4 Hz, 3H), 0.86 (s, 9H). ^{13}C NMR (100 MHz, DMSO-d_6) δ 168.4, 152.2, 140.8, 140.0, 136.1, 130.5,

129.2, 128.7, 125.8, 122.7, 122.3, 115.2, 111.0, 110.7, 70.8, 60.0, 52.5, 51.4, 34.0, 27.5, 26.2, 14.0; LC/MS: retention time 3.930 min (Gradient: 4% to 100% acetonitrile (0.05% TFA) over 7 min); HRMS: *m/z* ($M+H^+$) = 495.2538 (Calculated for $C_{26}H_{35}N_6O_2S$ = 495.2542).

Statistical analysis

Sample size for *in vivo* studies including inhibitor treatment and diabetes induction were estimated by conducting pilot experiments. No samples or animals were excluded from the analyses. For animal studies, no randomization and blinding were used. Data were analyzed using Prism statistical software. Normally and non-normally distributed data were analyzed for significance by Student's *t*-test and Mann-Whitney test respectively. The variance was similar between groups being compared. Standard error and p-values are shown on individual graphs.

Supplementary Material

Refer to Web version on PubMed Central for supplementary material.

Acknowledgments

We thank Drs. E. Huseby, B. Seed and R. Friedline for discussion, Dr. S. Turley for advice with stromal cells, Dr. T. Hunig for CD28SA antibody, Dr. M. Coles for microscopy, Dr. M. Krummel for advice on imaging, Dr. D. Serreze for studies with diabetogenic $CD8^+$ T cells, Dr. Huseby for mice and Dr. R. Welsh for LCMV infection protocol. Core resources supported by the DERC grant DK32520 were used. This work was supported by US NIH grants to DG (AI46629, AI050864), SLS (AI046530), LJB (AI083505) and JK (RC1 DK086474 and AI083505). US NIH Chemical Genomics Center was supported by the Molecular Libraries Initiative and the Intramural Research Program of the NHGRI.

References

1. Bour-Jordan H, et al. Intrinsic and extrinsic control of peripheral T-cell tolerance by costimulatory molecules of the CD28/ B7 family. Immunol Rev. 2011; 241:180–205. [PubMed: 21488898]
2. Harding F, McArthur JG, Gross JA, Raulet DH, Allison JP. CD28 mediated signalling costimulates murine T cells and prevents the induction of anergy in T cell clones. Nature. 1992; 356:607–609. [PubMed: 1313950]
3. Boise LH, et al. CD28 costimulation can promote T cell survival by enhancing the expression of bcl-xl. Immunity. 1995; 3:87–98. [PubMed: 7621080]
4. Frauwirth KA, et al. The CD28 signaling pathway regulates glucose metabolism. Immunity. 2002; 16:769–777. [PubMed: 12121659]
5. Marelli-Berg FM, Okkenhaug K, Mirenda V. A two-signal model for T cell trafficking. Trends Immunol. 2007; 28:267–273. [PubMed: 17481953]
6. Shimizu Y, et al. Crosslinking of the T cell-specific accessory molecules CD7 and CD28 modulates T cell adhesion. J Exp Med. 1992; 175:577–582. [PubMed: 1370688]
7. Michel F, et al. CD28 utilizes Vav-1 to enhance TCR-proximal signaling and NF-AT activation. J Immunol. 2000; 165:3820–3829. [PubMed: 11034388]
8. Salazar-Fontana LI, Barr V, Samelson LE, Bierer BE. CD28 engagement promotes actin polymerization through the activation of the small Rho GTPase Cdc42 in human T cells. J Immunol. 2003; 171:2225–2232. [PubMed: 12928366]
9. Kondo S, Kooshesh F, Wang B, Fujisawa H, Sauder DN. Contribution of the CD28 molecule to allergic and irritant-induced skin reactions in CD28 −/− mice. J Immunol. 1996; 157:4822–4829. [PubMed: 8943384]

10. Girvin AM, et al. A critical role for B7/CD28 costimulation in experimental autoimmune encephalomyelitis: A comparative study using costimulatory molecule-deficient mice and monoclonal antibody blockade. J Immunol. 2000; 164:136–143. [PubMed: 10605004]
11. Chang TT, Jabs C, Sobel RA, Kuchroo VK, Sharpe AH. Studies in B7-deficient mice reveal a critical role for B7 costimulation in both induction and effector phases of experimental autoimmune encephalomyelitis. J Exp Med. 1999; 190:733–740. [PubMed: 10477557]
12. Lenschow DJ, et al. CD28/B7 regulation of Th1 and Th2 subsets in the development of autoimmune diabetes. Immunity. 1996; 5:285–293. [PubMed: 8808683]
13. Salomon B, et al. B7/CD28 costimulation is essential for the homeostasis of the CD4+CD25+ immunoregulatory T cells that control autoimmune diabetes. Immunity. 2000; 12:431–440. [PubMed: 10795741]
14. Lenschow DJ, et al. Differential effects of anti-B7-1 and anti-B7-2 monoclonal antibody treatment on the development of diabetes in the nonobese diabetic mouse. J Exp Med. 1995; 181:1145–1155. [PubMed: 7532678]
15. Chambers CA, Kuhns MS, Egen JG, Allison JP. CTLA-4-mediated inhibition in regulation of T cell responses: mechanisms and manipulation in tumor immunotherapy. Ann Rev Immunol. 2001; 19:565–594. [PubMed: 11244047]
16. Greenwald RJ, Freeman GJ, Sharpe AH. The B7 family revisited. Ann Rev Immunol. 2005; 23:515–548. [PubMed: 15771580]
17. Gough SC, Walker LS, Sansom DM. CTLA4 gene polymorphism and autoimmunity. Immunol Rev. 2005; 204:102–115. [PubMed: 15790353]
18. Chambers CA, Sullivan TJ, Allison JP. Lymphoproliferation in CTLA-4-deficient mice is mediated by costimulation-dependent activation of CD4+ T cells. Immunity. 1997; 7:885–895. [PubMed: 9430233]
19. Ise W, et al. CTLA-4 suppresses the pathogenicity of self antigen-specific T cells by cell-intrinsic and cell-extrinsic mechanisms. Nat Immunol. 2010; 11:129–135. [PubMed: 20037585]
20. Wing K, et al. CTLA-4 control over Foxp3+ regulatory T cell function. Science (New York, N.Y. 2008; 322:271–275.
21. Friedline RH, et al. CD4+ regulatory T cells require CTLA-4 for the maintenance of systemic tolerance. J Exp Med. 2009; 206:421–434. [PubMed: 19188497]
22. Jain N, Nguyen H, Chambers C, Kang J. Dual function of CTLA–4 in regulatory T cells and conventional T cells to prevent multiorgan autoimmunity. Proc Natl Acad Sci U S A. 2010; 107:1524–8. [PubMed: 20080649]
23. Masteller EL, Chuang E, Reiner SL, Thompson CB. Structural analysis of CTLA-4 function in vivo. J Immunol. 2000; 164:5319–5327. A.C., M. [PubMed: 10799894]
24. Okkenhaug K, et al. A point mutation in CD28 distinguishes proliferative signals from survival signals. Nat Immunol. 2001; 2:325–332. [PubMed: 11276203]
25. Mirenda V, et al. Physiologic and aberrant regulation of memory T-cell trafficking by the costimulatory molecule CD28. Blood. 2007; 109:2968–2977. [PubMed: 17119120]
26. Michel F, Attal-Bonnefoy G, Mangino G, Mise-Omata S, Acuto O. CD28 as a molecular amplifier extending TCR ligation and signaling capabilities. Immunity. 2001; 15:935–945. [PubMed: 11754815]
27. Berg LJ, Finkelstein LD, Lucas JA, Schwartzberg PL. Tec family kinases in T lymphocyte development and function. Ann Rev Immunol. 2005; 23:549–600. [PubMed: 15771581]
28. Woods ML, et al. A novel function for the Tec family tyrosine kinase Itk in activation of beta 1 integrins by the T-cell receptor. EMBO J. 2001; 20:1232–1244. [PubMed: 11250890]
29. Takesono A, Horai R, Mandai M, Dombroski D, Schwartzberg PL. Requirement for Tec kinases in chemokine-induced migration and activation of Cdc42 and Rac. Curr Biol. 2004; 14:917–922. [PubMed: 15186750]
30. Fowell DJ, et al. Impaired NFATc translocation and failure of Th2 development in Itk-deficient CD4+ T cells. Immunity. 1999; 11:399–409. [PubMed: 10549622]
31. Mandelbrot DA, et al. B7-dependent T-cell costimulation in mice lacking CD28 and CTLA4. J Clin Invest. 2001; 107:881–887. [PubMed: 11285307]

32. Fletcher AL, et al. Lymph node fibroblastic reticular cells directly present peripheral tissue antigen under steady-state and inflammatory conditions. J Exp Med. 2010; 207:689–697. [PubMed: 20308362]
33. Lozanoska-Ochser B, Klein NJ, Huang GC, Alvarez RA, Peakman M. Expression of CD86 on human islet endothelial cells facilitates T cell adhesion and migration. J Immunol. 2008; 181:6109–6116. [PubMed: 18941200]
34. Perez VL, Henault L, Lichtman AH. Endothelial antigen presentation: stimulation of previously activated but not naive TCR-transgenic mouse T cells. Cell Immunol. 1998; 189:31–40. [PubMed: 9758692]
35. Kreisel D, et al. Mouse vascular endothelium activates CD8+ T lymphocytes in a B7-dependent fashion. J Immunol. 2002; 169:6154–6161. [PubMed: 12444119]
36. Thornton EE, et al. Spatiotemporally separated antigen uptake by alveolar dendritic cells and airway presentation to T cells in the lung. J Exp Med. 2012; 209:1183–1199. [PubMed: 22585735]
37. Ledgerwood LG, et al. The sphingosine 1-phosphate receptor 1 causes tissue retention by inhibiting the entry of peripheral tissue T lymphocytes into afferent lymphatics. Nat Immunol. 2008; 9:42–53. [PubMed: 18037890]
38. Cahalan MD, Parker I. Choreography of cell motility and interaction dynamics imaged by two-photon microscopy in lymphoid organs. Ann Rev Immunol. 2008; 26:585–626. [PubMed: 18173372]
39. Sanderson MJ. Exploring lung physiology in health and disease with lung slices. Pulm Pharmacol Ther. 2011; 24:452–465. [PubMed: 21600999]
40. Dennehy KM, et al. Cutting edge: monovalency of CD28 maintains the antigen dependence of T cell costimulatory responses. J Immunol. 2006; 176:5725–5729. [PubMed: 16670276]
41. Goverman J, Brabb T, Paez A, Harrington C, von Dassow P. Initiation and regulation of CNS autoimmunity. Crit Rev Immunol. 1997; 17:469–480. [PubMed: 9419434]
42. Liu L, Callahan MK, Huang D, Ransohoff RM. Chemokine receptor CXCR3: an unexpected enigma. Curr Top Dev Biol. 2005; 68:149–181. [PubMed: 16124999]
43. Burkhardt JK, Carrizosa E, Shaffer MH. The actin cytoskeleton in T cell activation. Ann Rev Immunol. 2008; 26:233–259. [PubMed: 18304005]
44. Readinger JA, et al. Selective targeting of ITK blocks multiple steps of HIV replication. Proc Natl Acad Sci U S A. 2008; 105:6684–6689. [PubMed: 18443296]
45. Lin TA, et al. Selective Itk inhibitors block T-cell activation and murine lung inflammation. Biochem. 2004; 43:11056–11062. [PubMed: 15323564]
46. Riether D, et al. 5-Aminomethylbenzimidazoles as potent ITK antagonists. Bioorg Med Chem Lett. 2009; 19:1588–1591. [PubMed: 19246196]
47. Peterson JD, Haskins K. Transfer of diabetes in the NOD-scid mouse by CD4 T-cell clones. Differential requirement for CD8 T-cells. Diabetes. 1996; 45:328–336. [PubMed: 8593938]
48. Bachmann MF, et al. Normal responsiveness of CTLA-4-deficient anti-viral cytoxic T cells. J Immunol. 1998; 160:95–100. [PubMed: 9551960]
49. Shahinian A, et al. Differential T cell costimulatory requirements in CD28-deficient mice. Science (New York, N.Y. 1993; 261:521–652.
50. Collins AV, et al. The interaction properties of costimulatory molecules revisited. Immunity. 2002; 17:201–210. [PubMed: 12196291]
51. Yokosuka T, et al. Spatiotemporal basis of CTLA-4 costimulatory molecule-mediated negative regulation of T cell activation. Immunity. 2010; 33:326–339. [PubMed: 20870175]
52. Puccetti P, Grohmann U. IDO and regulatory T cells: a role for reverse signalling and non-canonical NF-kappaB activation. Nat Rev Immunol. 2007; 7:817–823. [PubMed: 17767193]
53. Qureshi OS, et al. Trans-endocytosis of CD80 and CD86: a molecular basis for the cell-extrinsic function of CTLA-4. Science (New York, N.Y. 2011; 332:600–603.
54. Bachmann MF, Littman DR, Liao XC. Antiviral immune responses in Itk-deficient mice. J Virol. y. 1997; 71:7253–7257.

55. Orban T, et al. Co-stimulation modulation with abatacept in patients with recent-onset type 1 diabetes: a randomised, double-blind, placebo-controlled trial. Lancet. 2011; 378:412–419. [PubMed: 21719096]

56. Bauer M, et al. Beta1 integrins differentially control extravasation of inflammatory cell subsets into the CNS during autoimmunity. Proc Natl Acad Sci U S A. 2009; 106:1920–1925. [PubMed: 19179279]

57. Dombroski D, et al. Kinase-independent functions for Itk in TCR-induced regulation of Vav and the actin cytoskeleton. J Immunol. 2005; 174:1385–1392. [PubMed: 15661896]

58. Guo W, et al. Molecular characteristics of CTA056, a novel interleukin-2-inducible T-cell kinase inhibitor that selectively targets malignant T cells and modulates oncomirs. Mol Pharmacol. 2012; 82:938–947. [PubMed: 22899868]

59. McCausland MM, Crotty S. Quantitative PCR technique for detecting lymphocytic choriomeningitis virus in vivo. J Virol Methods. 2008; 147:167–176. [PubMed: 17920702]

60. McKinstry KK, et al. IL-10 deficiency unleashes an influenza-specific Th17 response and enhances survival against high-dose challenge. J Immunol. 2009; 182:7353–7363. [PubMed: 19494257]

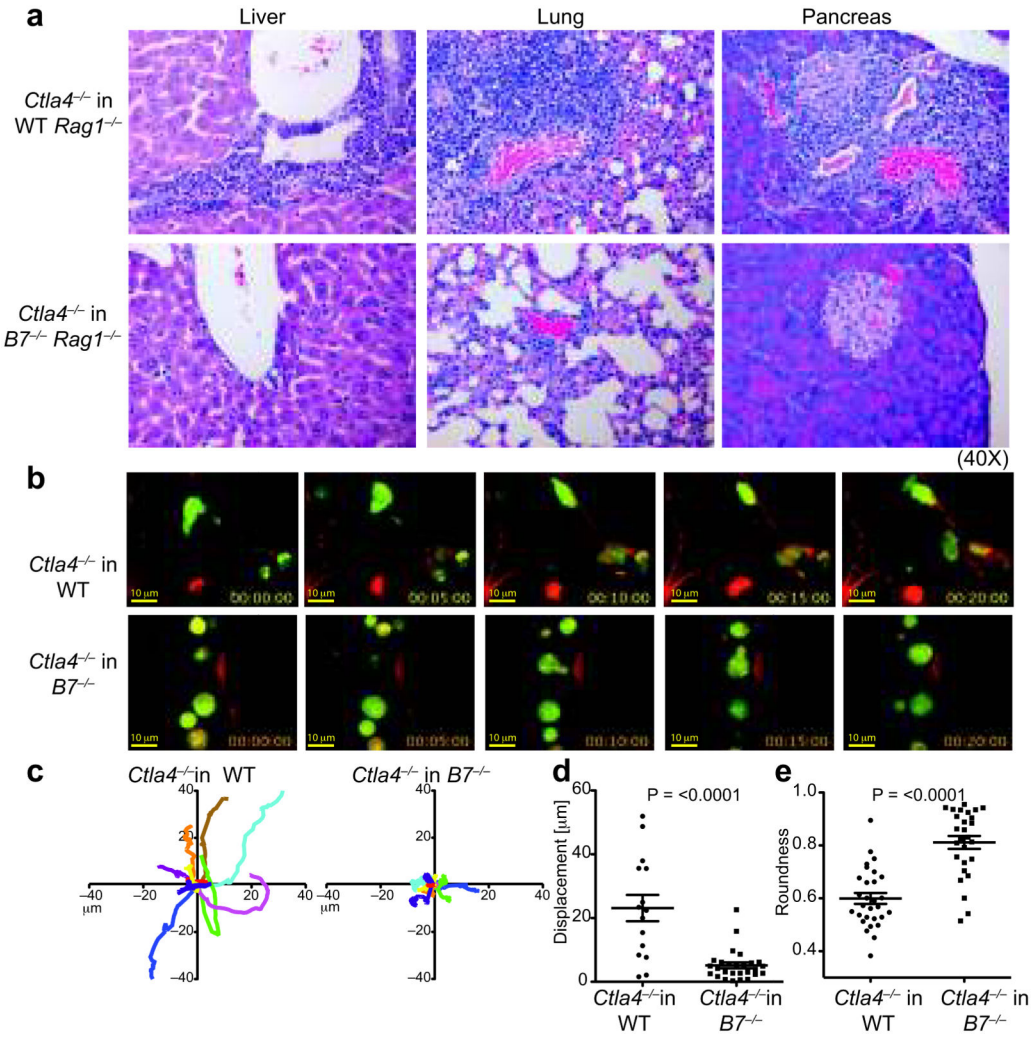

Figure 1. B7 signals regulate *Ctla4*$^{-/-}$ T cell migration

a. H&E sections of tissues from *Rag1*$^{-/-}$ and B7$^{-/-}$*Rag1*$^{-/-}$ mice 3 weeks after transfer of *Ctla4*$^{-/-}$ T cells. Data are representative of ≥3 experiments with 4-6 mice in each group. **b-e.** Imaging of CFSE labeled *Ctla4*$^{-/-}$ T cells in lung vasculature of WT or B7$^{-/-}$ mice **b.** Representative frames (0-20 minutes) from a Video Savant movie recording showing T cell movement (green) in blood vessels (red) of lung slices. **c.** 2-D tracks of 10 representative T cells within blood vessels (in 10 minutes), superimposed after normalizing their starting coordinates to the origin. A minimum of 30 cells was analyzed for each genotype. Scale: 0.18 microns pixel^{-1}. **d.** Displacement of individual *Ctla4*$^{-/-}$ T cells in WT or B7$^{-/-}$ lungs from the point of origin in 10 minutes. **e.** Roundness of cells as calculated by ImageJ (NIH) software. 1= circular object; <1: decreasing circularity. Data in **d** and **e** show mean and SEM, p values in **d** and **e** based on the Mann-Whitney and Student's *t*-test, respectively.

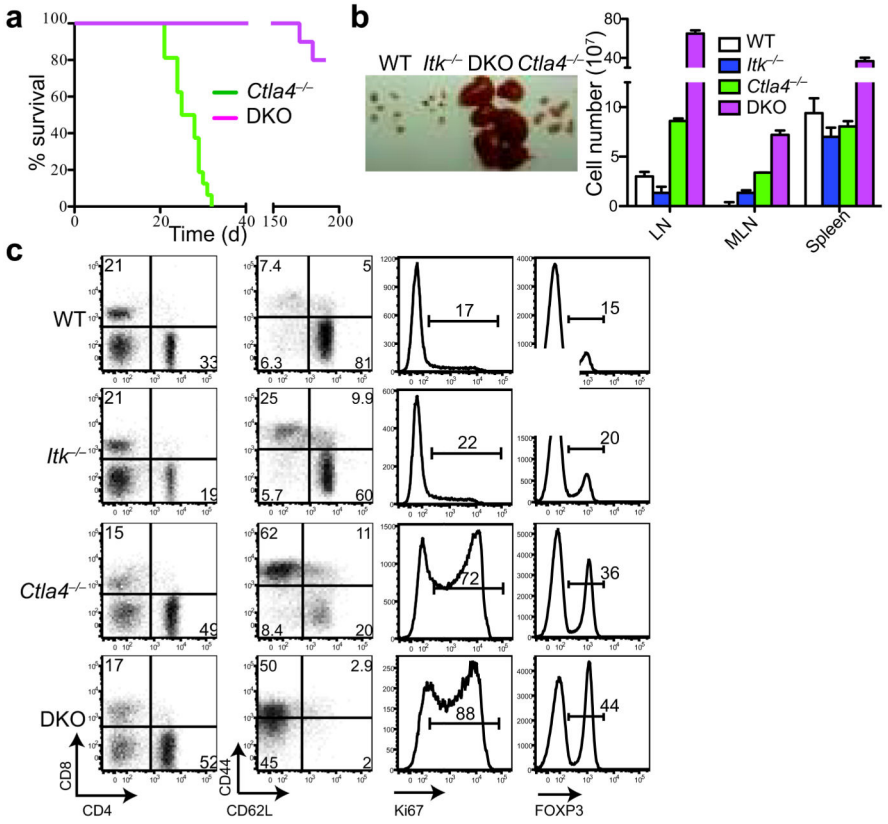

Figure 2. ITK deficiency prolongs lifespan of *Ctla4*$^{-/-}$ mice

a. Survival curves of *Ctla4*$^{-/-}$ (n=10) and *Itk*$^{-/-}$*Ctla4*$^{-/-}$ (DKO) (n=10) mice. P-value =<0.0001 (Log-rank Mantel-Cox test) **b.** (*Left*) Size of peripheral (inguinal, axial and brachial) LNs. (*Right*) Cell numbers in peripheral LNs, mesenteric LNs (MLN) and spleen of 3 weeks old *Ctla4*$^{-/-}$ and 6-8 weeks old WT, *Itk*$^{-/-}$ and DKO mice. **c.** *(From left to right*) Frequencies of CD4^{+}/CD8^{+} T cells, CD4^{+} Tconv cells expressing activation markers CD44/CD62L, CD4^{+} Tconv cells expressing Ki67, and Treg cells in LNs of indicated mice as in **b**. Data in **b** and **c** are representative of 3 experiments with ≥4 mice in each group.

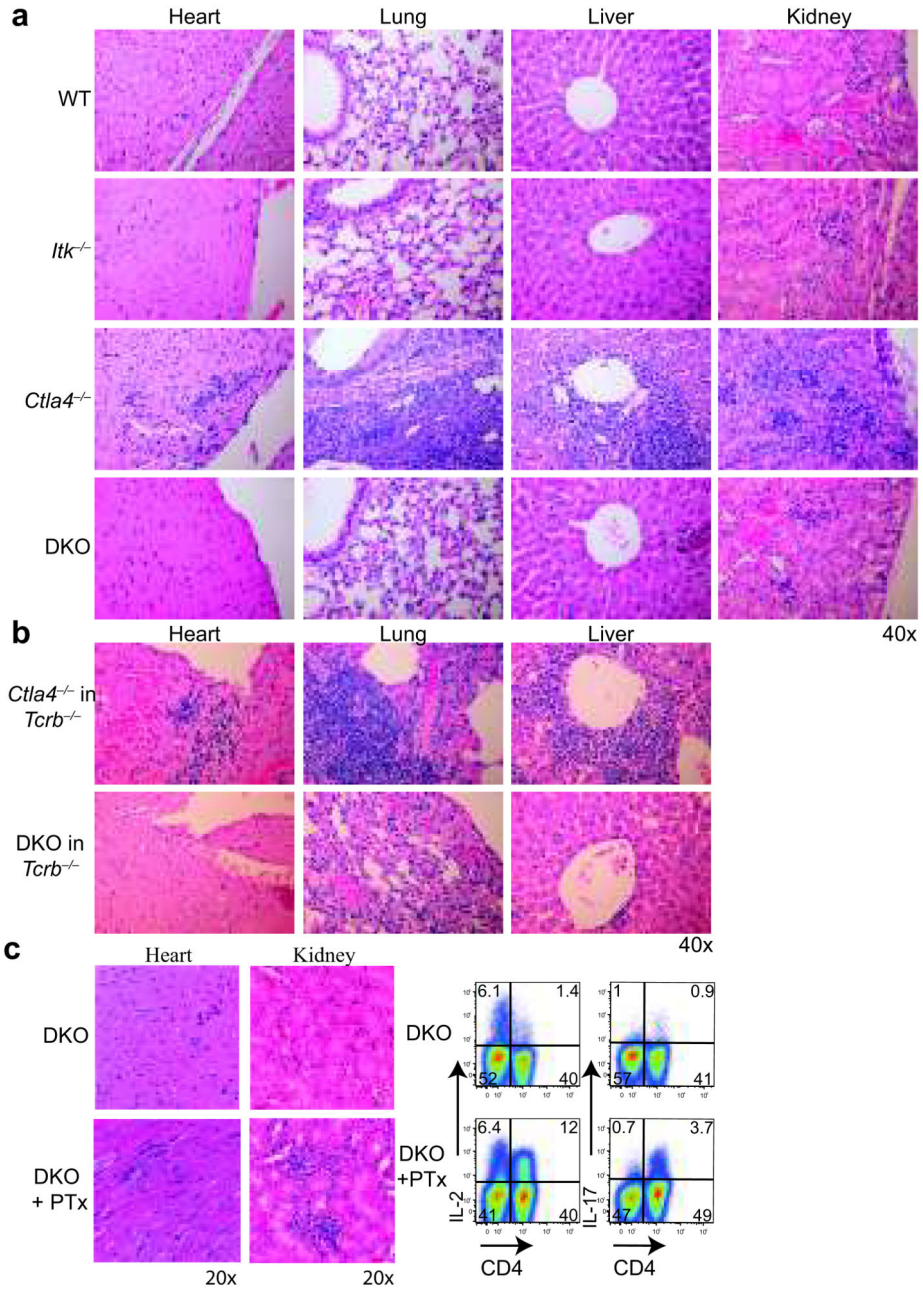

Figure 3. ITK deficiency prevents *Ctla4*$^{-/-}$ T cell infiltration into tissues

H&E sections of tissues from **a.** 3 weeks old *Ctla4*$^{-/-}$ and 8-12 weeks old WT, *Itk*$^{-/-}$ and DKO mice, and **b**. *Tcrb*$^{-/-}$ mice 4 weeks post-transfer of 10^7 CD4$^+$ T cells from *Ctla4*$^{-/-}$ and DKO mice. **c.** (*Left*) H&E sections of tissues 8 weeks after PTX treatment of DKO mice. (*Right*) Flow cytometry profiles of *ex vivo* IL-2 and IL-17 production by LN CD4$^+$ T cells from PTX-DKO mice. Data are representative of 3 independent experiments with ≥4 mice in each group.

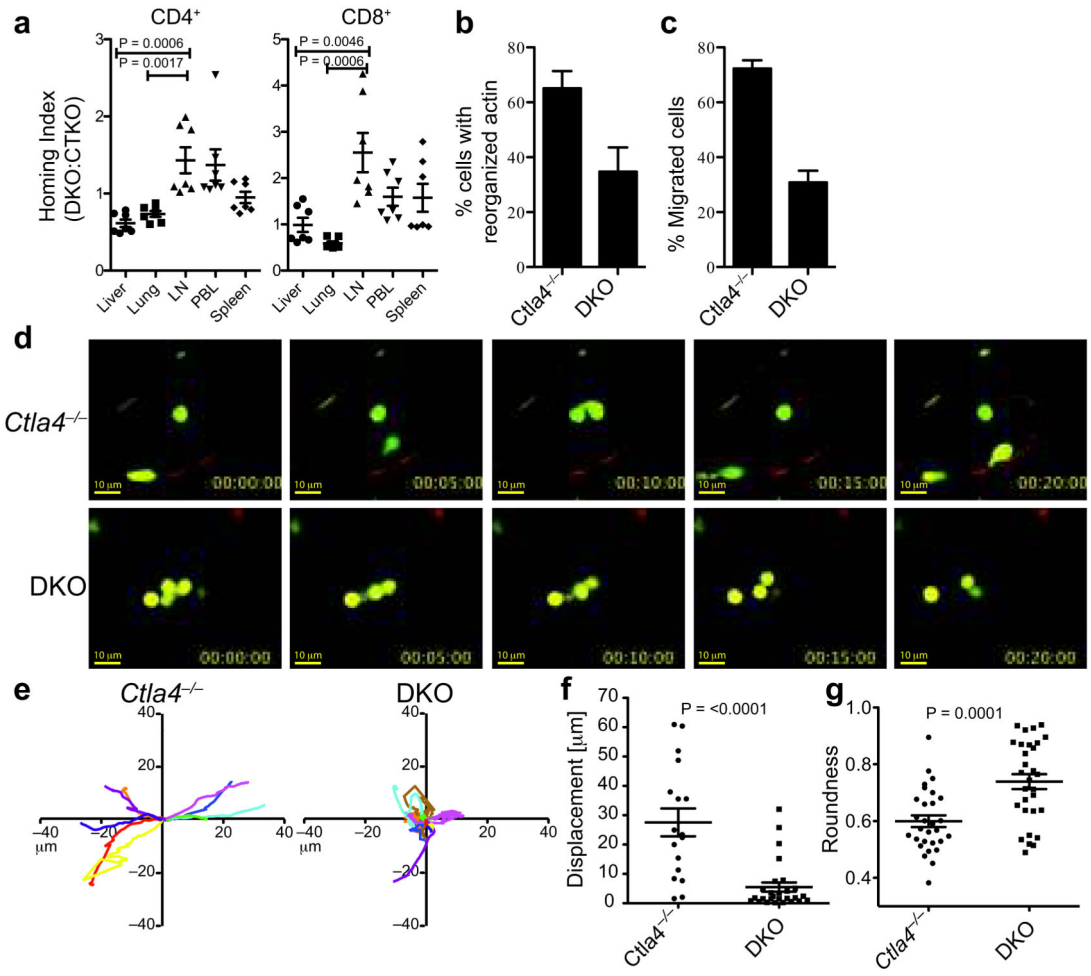

Figure 4. Impaired trans-EC migration by DKO T cells

a. HI of eFluor670-labeled *Ctla4*$^{-/-}$ and CFSE-labeled DKO CD4^{+} and CD8^{+} T cells in indicated organs 6-8 hours post-transfer into female *Rag1*$^{-/-}$ mice. HI was calculated as the ratio of CFSE:eFluor670 in tissues normalized to the ratio of CFSE:eFluor670 T cells injected into the host. Data are combined from 2 independent experiments, each with 3-4 recipients/group. **b.** Frequency of CD4^{+} T cells with polarized F-actin in the LNs and spleens of *Ctla4*$^{-/-}$ and DKO mice. Data are from 3 experiments with at least 300 cells analyzed for each genotype. **c.** Frequency of *Ctla4*$^{-/-}$ and DKO CD4^{+} T cell migration (diapedesis) across SVEC4-10 ECs. Data are representative of 4 experiments. **d-g.** Imaging of LN T cells from *Ctla4*$^{-/-}$ and DKO mice in lung vasculature of *Rag1*$^{-/-}$ mice **d.** Representative frames (0-20 minutes) from a Video Savant movie recording showing movement of T cells (CFSE, green) in blood vessels (red) of lung slices. **e.** 2-D tracks of 10 representative T cells within blood vessels (in 10 minutes), superimposed after normalizing their starting coordinates to the origin. A minimum of 40 cells was analyzed/genotype. Scale: 0.18 microns pixel^{-1}. **f.** Displacement of *Ctla4*$^{-/-}$ and DKO T cells from the point of origin. **g.** Shape of *Ctla4*$^{-/-}$ and DKO T cells within blood vessels in lung slices (1= circular cell, <1= elongated cell). Data in **d-g** are from 6 experiments. Data in **a-c** and **f, g** show mean, SEM and *p*-values (Student's *t*-test).

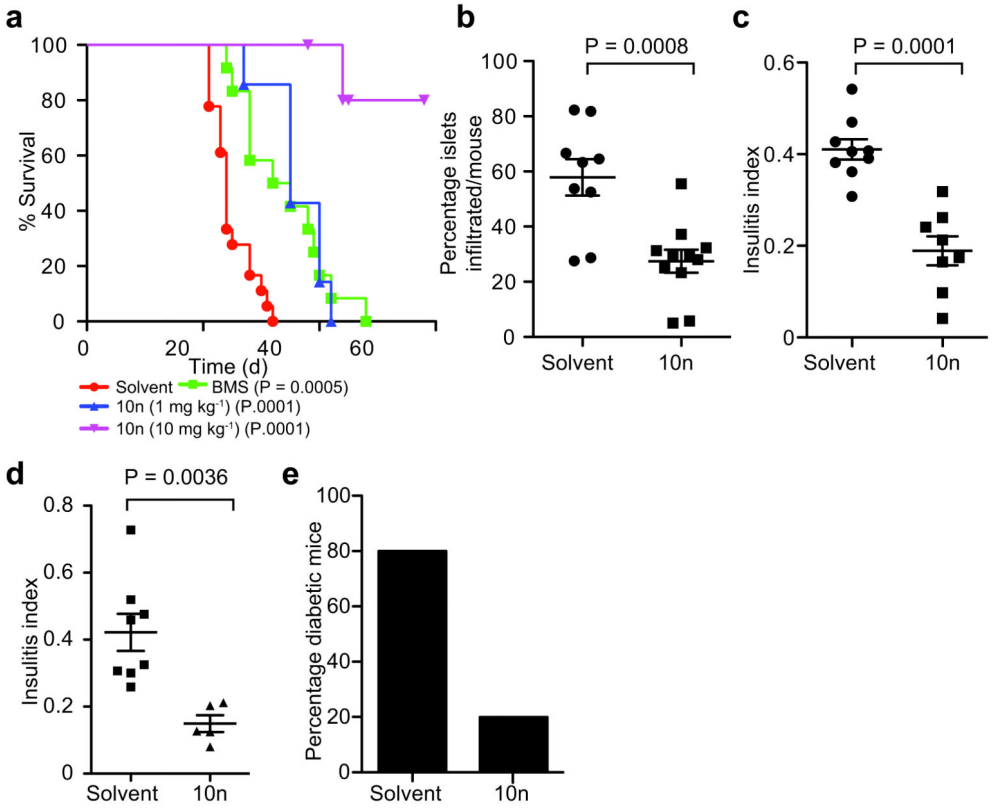

Figure 5. ITK inhibitors modulate autoimmunity

a. Survival curves of *Ctla4*$^{-/-}$ mice (10 days old) that were treated with ITK inhibitors, BMS509744 (50mg kg^{-1}, n=11), and 10n (1mg kg^{-1}, n=8; and 10mg kg^{-1}, n=5), and solvent alone (n=10). P-values shown based on the Log-rank Mantel-Cox test. **b.** Frequency of islets infiltrated and **c.** the insulitis index of 8 weeks old female NOD mice treated with 10n (1mg/kg from 5 weeks of age). Data from 3 experiments with 4-10 mice per group/experiment. **d, e.** CD4^{+} Tconv cells from BDC2.5/NOD mice were transferred into NOD/*Scid* mice followed by 10n treatment at 1mg kg^{-1}. **d.** Insulitis index and **e.** frequency of diabetic mice. Data are from 3 experiments with 10 and 5 mice in control and 10n treated, respectively.